

ARTICLE OPEN



Global increase in destructive potential of extratropical transition events in response to greenhouse warming

Hung Ming Cheung ¹ and Jung-Eun Chu ^{1,2}✉

When tropical cyclones (TCs) move to the mid-latitudes, they oftentimes undergo extratropical transition (ET) by which they lose their symmetry and warm-core characteristics. Upon transforming into extratropical cyclones (ETCs), they tend to impact larger areas and thus larger populations. In light of the increased TC intensity due to global warming identified in previous studies, here we examine its effect on the frequency and destructiveness of ET events globally using a high-resolution fully coupled Earth System model (0.25° for atmosphere; 0.1° for ocean) prescribed with present-day, doubling, and quadrupling CO₂ concentrations. Our findings indicate that ETCs originated from the tropics with higher destructiveness (indicated by integrated kinetic energy) become more frequent in response to greenhouse warming, although the number of ET events does not change significantly. The key factor in the change in the destructiveness of ETCs is the increase in wind speed and the high-wind area at ET. Despite the uncertainty in the Northern Hemisphere, our results underscore the necessity for climate resilience in the mid-latitudes against global warming.

npj Climate and Atmospheric Science (2023)6:137; <https://doi.org/10.1038/s41612-023-00470-8>

INTRODUCTION

Extratropical transition (ET) is a process related to the changes in properties of tropical cyclones (TCs), which are one of the most devastating natural phenomena on Earth. During the transition, a TC gradually transforms from a symmetric and warm-core structure to an asymmetric and cold-core structure, and also gains energy from the strong temperature and moisture gradient instead of the water vapor evaporated over warm water^{1–3}. Environments conducive to ET include lower sea-surface temperature (SST), steeper SST gradient, less moisture, and stronger vertical wind shear, which are common in the extratropics^{4–7}. If a TC does not dissipate before the transition is completed, it becomes an extratropical cyclone (ETC) that usually possesses greater translational speed and spatial coverage than its tropical predecessor^{4,8}. For the ETCs which impact Europe, the maximum intensity of those with tropical origin can be significantly greater than those that form in the mid-latitudes⁹. A transitioning TC can also exert an impact far away from it. For example, the ET of Supertyphoon Nuri (2014), which was active in the West Pacific, indirectly led to heavy precipitation, cold-air outbreak, and heat wave in different parts of the US¹⁰. As a result, TCs which undergo or complete transition can pose a serious threat to both the inland and coastal populations outside the tropics.

Although a TC is regarded as weakening when it moves to the mid-latitudes, transitioning or transitioned storms can still be accompanied by strong wind and heavy precipitation⁴ and sometimes re-intensify during the transition. Hurricane Sandy, which formed in late October 2012 over the southern Caribbean, completed ET before its landfall at New Jersey of the US East coast as a Category 1 TC under the Saffir–Simpson scale¹¹. Despite being a relatively weakened storm, its hurricane-force wind extended as far as 280 km from the storm center¹². Therefore, the storm surge induced by Sandy affected an extended coastline across New Jersey and New York, with the highest surge reaching 9–10 feet. Compound with the astronomical high tides, it caused a death toll of 72 and the associated property damage exceeded \$50 billion

US dollars¹³. Hurricane Ophelia (2017) is another storm which made a severe impact after the ET completion. It struck Ireland as an ETC after its formation in the North Atlantic Ocean, and it remained over the ocean during its tropical phase^{14,15}. Flooding, fallen trees, and electricity poles/cables caused widespread damage, as well as three deaths in Ireland. In the West Pacific, Typhoon Hagibis (2019) began ET in October before making landfall in Japan¹⁶. During the transition, the daily rainfall record in the country was broken at the Hakone station (922.5 mm)¹⁷ and caused over 90 deaths, 465 injuries, and almost 80,000 houses flooded or damaged¹⁸. Moreover, extreme ETCs can cause damage to forests^{19,20} and coastal infrastructure²¹, and endanger marine traffic^{22,23}. The changes in ET activities in the future therefore bear high importance due to the socioeconomic impact.

Under a warmer climate, we expect a potential increase in the mean or maximum TC intensity^{24–28}, so the possibility of TCs surviving a prolonged period beyond the tropics or subtropics becomes greater. In recent years, several studies have focused on the possible future changes in ET activities caused by anthropogenic warming using climate models. Multiple studies have shown increases in the number of ET events or ET fraction over the North Atlantic Ocean using global models^{29–31}, although several high-resolution models from phase 6 of the Coupled Model Intercomparison Project (CMIP6) High-Resolution Model Intercomparison Project (HighResMIP³²) show mixed results in spatial distribution³³. Future increases in storm intensity during ET^{34,35}, or at ET completion and after³⁰ are also documented. Consequently, the proportion of transitioning TCs affecting Europe can also increase³⁶. However, in terms of global changes in ET activities, basins other than the North Atlantic received relatively less attention^{31,33}. There are diverse results for the ET frequency or fraction over the West Pacific, South Indian, and South Pacific^{30,31,33}. In addition to the lack of investigation on a global scale, the use of high-resolution fully coupled global models, which enable mesoscale atmospheric and oceanic features to be

¹School of Energy and Environment, City University of Hong Kong, Hong Kong, China. ²Low-Carbon and Climate Impact Research Centre, School of Energy and Environment, City University of Hong Kong, Hong Kong, China. ✉email: jungeun.chu@cityu.edu.hk

resolved and is essential for improved simulation of TC activities, for studying future changes in ET events is rare³³.

ET is unlikely if a storm is too weak to reach the mid-latitudes. Given that TC is the pre-requisite of any ET event, we can expect that improvement in TC simulation should have a positive influence on that of ET. Previous studies have shown that the horizontal resolution of a model has an impact on the simulation of TC activities. Roberts et al.³⁷ assessed the role of horizontal resolution by evaluating six pairs of global climate models with greater (50–200 km) and smaller (25–50 km) grid spacing from the HighResMIP project. By comparing model simulations with observation, they concluded that increased model resolution could improve the spatial distribution of TC tracks and enable more intense TC to be simulated, although only one of them can simulate TC stronger than Category 3. Furthermore, coupling atmospheric model with ocean model can improve the simulation of air–sea interaction and thus TC activities such as TC peak intensity³⁸ and TC genesis frequency³⁹ compared to an atmosphere-only model, as the strong surface wind of TC can trigger both positive and negative feedback by enhancing evaporation⁴⁰ and sea-surface cooling⁴¹, respectively. Moreover, Baker et al.³³ utilized the models in the HighResMIP project to demonstrate that the ensemble model bias in track density of TC that undergo ET in the North Atlantic and West Pacific is reduced when the model grid spacing decreases.

To improve the prediction of the potential risk induced by ET events in the future, here we analyze the global changes in ET activities under increased CO₂ concentration scenarios simulated by a high-resolution fully coupled global climate model, with a focus on destructiveness (also as destructive potential). The intensity of a TC or ETC (maximum sustained wind speed or mean sea level pressure at storm center) is commonly used for indicating its potential for causing damage. However, given the asymmetric nature and expanded wind field of the ETCs, storm intensity is not a sufficient indicator of destructiveness. Instead, we use integrated kinetic energy (IKE) that measures both the intensity and the extent of the wind field covered by a storm. The use of a high-resolution version for both the atmosphere (0.25°) and ocean components (0.1°) of the Community Earth System Model (CESM) allows an improved simulation of mesoscale oceanic features²⁴, which is important for the sensitivity of TC frequency⁴². This model resolution is close to the finest one (0.25° for the atmosphere and 0.05° for the ocean, but in separate models) among the models participating in HighResMIP³² and those in ref. ³³. We apply the cyclone phase space which illustrates the structural evolution of a TC to characterize ET events. The results suggest an increase in the proportion or frequency of highly destructive transitioned TCs, together with a decrease in the total number of TCs, as a result of greenhouse warming.

RESULTS

Simulated ET events in the present-day climate

We utilize three sets of model simulations for the study: present-day climate (PD), doubling (2×CO₂), and quadrupling CO₂ concentrations (4×CO₂) (see “Methods”). We select a model TC to demonstrate the capacity of the model to produce a realistic ET event. In the present study, an ET event is sub-divided into ET onset and completion based on the cyclone phase diagram (see “Methods”). ET onset is defined as the first time step at which a TC becomes either asymmetric or acquires cold-core structure, while the first time step at which a TC develops into a storm with both asymmetry and cold-core structure after onset is regarded as ET completion. The example shown in Fig. 1 is a typical TC formed in the West Pacific during the 133rd year of the PD simulation. It forms over the tropical ocean, moves northwestwards, and recurves towards the mid-latitudes (Fig. 1a). Its evolution also

follows a classical ET pathway on the cyclone phase diagram (see “Methods”): first becomes asymmetric (upper right quadrant) and then acquires a cold-core structure (upper left quadrant) (Fig. 1b). At the peak intensity of TC (Time 1), the 10-m wind field shows a high degree of symmetry in the vicinity of the inner core (Fig. 1c), and the precipitation is also the heaviest in that region (Fig. 1d). The maximum wind speed and rain rate are 61 m s⁻¹ and 1322 mm day⁻¹, respectively. The ET onset begins when the TC moves to the south of Japan (Time 2). The storm is much weaker than that at Time 1 with lower wind speed (43 m s⁻¹) and less precipitation (727 mm day⁻¹) over the inner-core region (Fig. 1e, f). The wind field at the ET onset started to become asymmetric and that of the TC outer region stretches zonally, expanding the influence of its high wind speeds. At the end of the ET (ET completion, Time 3), the maximum wind speed (28 m s⁻¹) and precipitation (63 mm day⁻¹) reduce further, and symmetry can no longer be observed from both fields (Fig. 1g, h). The result shows that CESM can replicate the actual evolution of a TC that undergoes ET.

We compare the transitioned TCs in the last 20 years of the PD simulation with the historical TC dataset from the International Best Track Archive for Climate Stewardship (IBTrACS⁴³). To align the period of observation data with the PD simulation which is based on a 2000-year greenhouse gas condition (367 ppm), we selected the 1991–2010 period. In general, the CESM can capture genesis (also as formation) location and TC tracks (both ET and non-ET events) well (Fig. 2a–d and Supplementary Fig. 1a, b). Active regions of TC activity (high TC passage frequency) in the PD simulation correspond with those in the observation. There is an underestimation of ET events in the West Pacific (0°–50°N, 100°–180°E), North Atlantic (0°–50°N, 10°–100°W), and South Indian (0°–50°S, 30°–135°E), while the model overestimates it over the South Pacific (0°–50°S, 135°E–70°W) (Figs. 2a–d and 3 and Supplementary Table 1). The smaller number of ET events over the North Atlantic is likely to be caused by a lack of TCs formed over the tropical ocean in the region, which is also exhibited in many global climate models^{24,37,44,45}. The shorter observed tracks compared to the simulated ones over the South Indian is because the area of responsibility of the meteorological center for this basin is limited to 40°S on the polar flank (Supplementary Fig. 1a, b). In addition, the maximum sustained wind speed during the ETC phase is mostly not recorded in the data from the Joint Typhoon Warning Center (JTWC), and it creates a discrepancy in storm intensity between the best track data and model output over the extratropics in the West Pacific and South Indian. For the seasonal cycle of TC and ET activity (insets in Supplementary Fig. 1), the model shows a distinctive TC season for all ocean basins. The temporal distribution of ET activity approximately follows that of TC. The peak of simulated ET activity is delayed by one month relative to the observation in the West Pacific, North Atlantic, and South Indian, while the model and observed peak align in the South Pacific.

The fraction of TCs that undergo ET is 25% globally which is contributed from about 40% in the North Atlantic and West Pacific, 20% in the South Indian, and 8% in the South Pacific Ocean (Fig. 3). The PD simulation tends to underestimate ET fraction in most of the basins except for South Pacific. Note that the observed fractions reported in other studies have a large variation depending on the datasets and methods used for defining ET. For example, it ranges from 27 to 65% in the West Pacific and 35 to 68% in the North Atlantic^{1,4,29,30,46–50}. The same is also true for simulated fractions. The ET fractions are 30–70% in the North Atlantic (six models^{29–31,46}), 32% or 50% in the West Pacific (two models^{30,31}), and at least 25% in other basins (one model³¹). In any case, we can see that the ET fraction in our study is lower, and the uncertainty among different models and methodologies is very high (especially outside the North Atlantic and West Pacific due to a lack of modeling study).

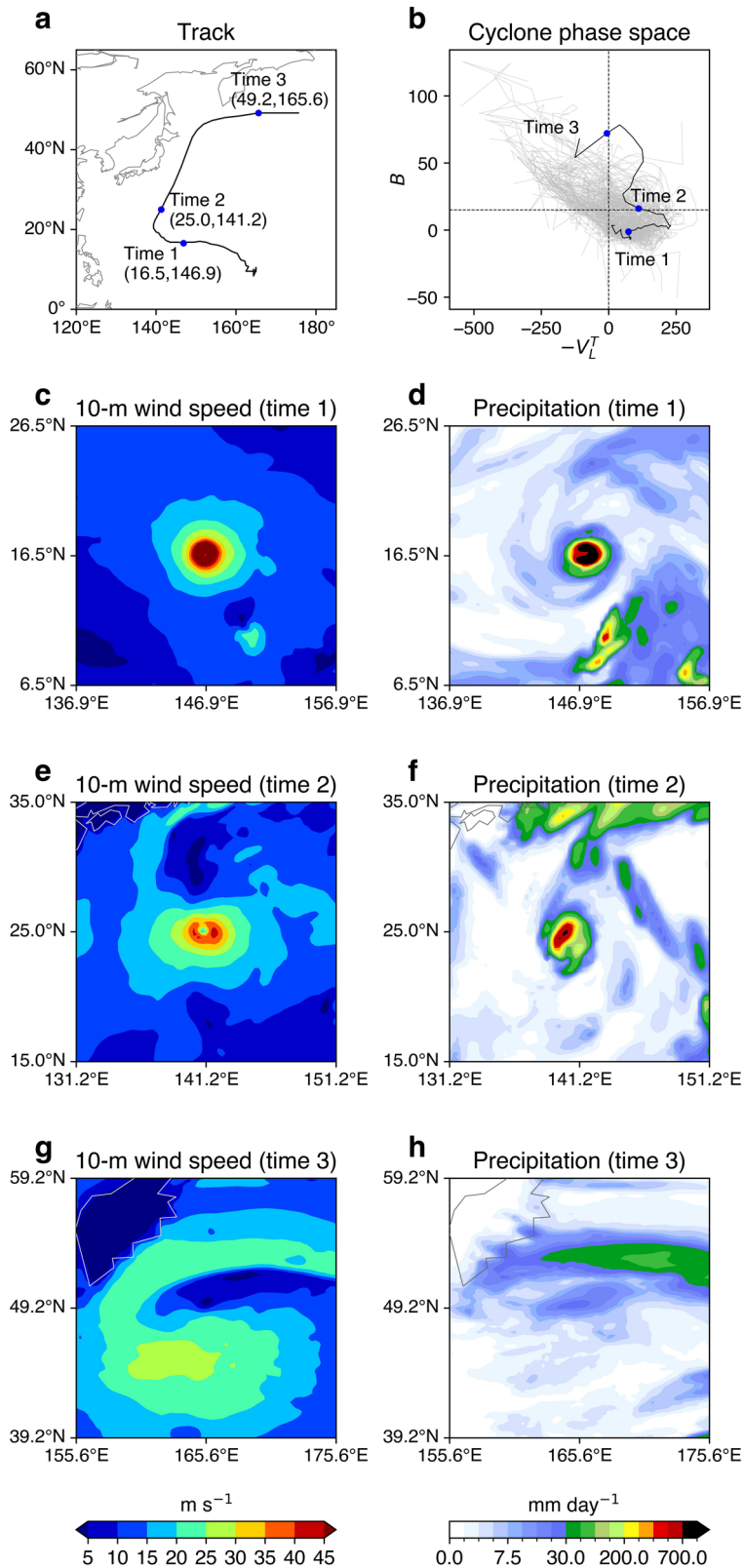


Fig. 1 An example of a transitioned tropical cyclone (TC) from the present-day simulation. **a** The track of the selected case. Blue circles correspond to the location of lifetime maximum intensity (Time 1), ET onset (Time 2), and ET completion (Time 3). The storm center (latitude and longitude in degrees North and East, respectively) at each time is displayed in the parenthesis. **b** The cyclone phase space depicting the evolution of the selected case (black line) and other TCs (gray lines) in the present-day simulation. **c–h** The 10-m wind speed (left) and precipitation (right) field of the storm at Times 1–3, centered at the storm center at the respective time.

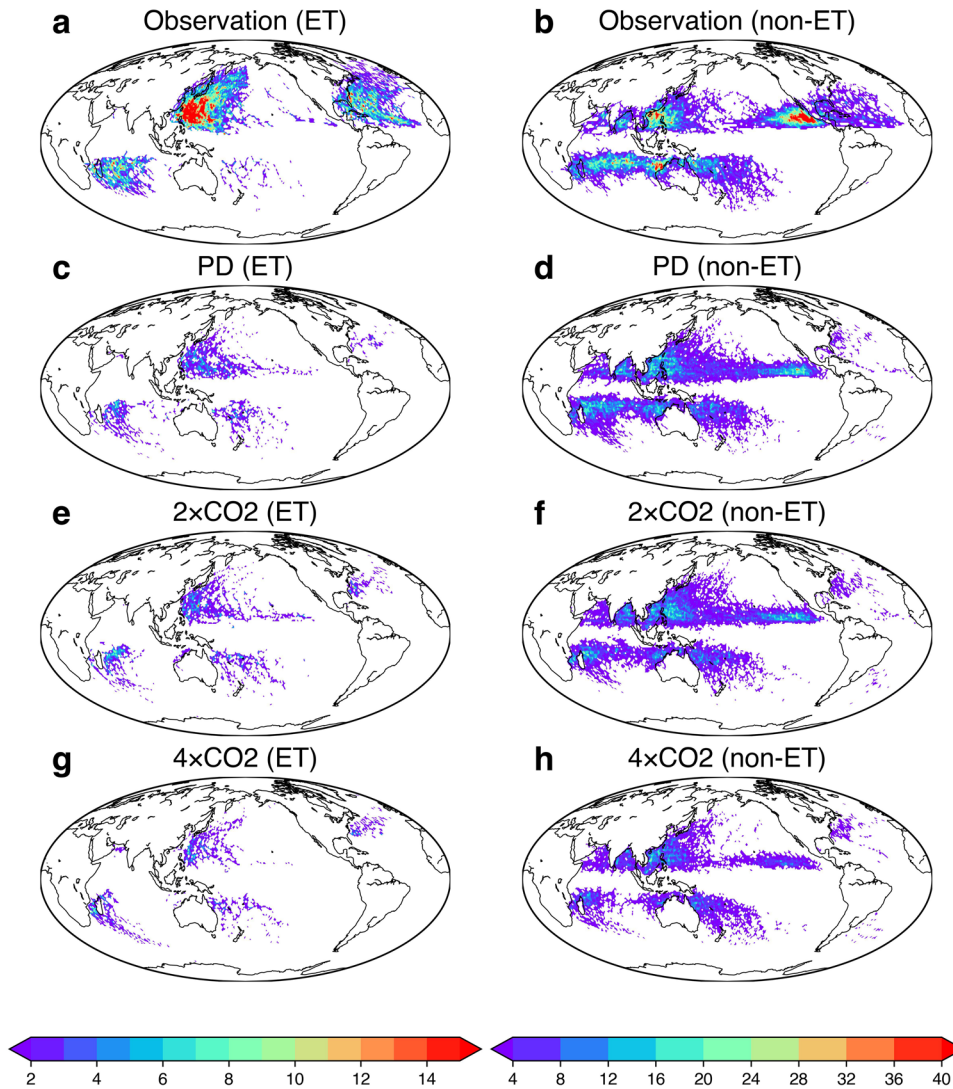


Fig. 2 Global distribution of tropical cyclones (TCs) track frequency with and without extratropical transition (ET) in historical data and climate simulations. The left- and right-hand column shows the ET and non-ET events, respectively, for **a, b** the observation; **c, d** the present-day simulation; **e, f** doubling CO_2 ; and **g, h** quadrupling CO_2 experiment. Each 6-hourly occurrence of storms is counted on a $1^\circ \times 1^\circ$ grid.

In the North Indian (0° – 50°N , 45° – 100°E) and East Pacific (0° – 50°N , 100° – 180°W), ET events rarely occur in the observation (1 and 6 times) and the PD simulation (2 and 17 times) (Supplementary Table 1). Considering the lesser contribution of ET events from these two ocean basins in observation and all simulations, we focus on the other basins in the following analyses. Furthermore, considering the large model bias in TC and ET frequency (notably the North Atlantic and West Pacific), we interpret the result in terms of the direction of change (increase or decrease).

Change in ET activity due to increased CO_2 concentration

To understand the changes in ET activity in response to global warming, we investigate the changes in TC and ET frequency, the fraction of ET to total TC (the sum of ET and non-ET events) (Fig. 3 and Supplementary Table 1), and intensity (Fig. 4) over each basin from the three experiments. Globally, there is a decrease in TC frequency under greenhouse warming. For the $2 \times \text{CO}_2$ experiment, a considerable reduction in TC frequency can be seen in the South Indian, while the changes in the other basins are little. However, a decrease in all basins is observed for the $4 \times \text{CO}_2$ experiment. The weakening of the rising branch of the Hadley Cell

during summer can be attributed to the decrease in TC frequency²⁴. The result is in agreement with Roberts et al.⁵¹ which shows that the majority of the models in HighResMIP predict TC frequency to decrease in the future.

The global or basin-wise frequency of ET events does not exhibit significant changes with CO_2 concentration (Fig. 3 and Supplementary Table 1). The changes in TC frequency mainly affect non-ET events. Statistically significant changes in the annual average number of ET events are not detected both in the $2 \times \text{CO}_2$ or $4 \times \text{CO}_2$ experiments relative to the PD simulation, and in any ocean basin. Previous studies generally showed increases in ET fraction in future simulations^{29–31}. To identify the linkage between changes in large-scale environments and the ET frequency, we calculate the maximum Eady growth rate in the active ET seasons to represent the regions of baroclinic development (Supplementary Fig. 2). Values of Eady growth rate greater than 0.25 day^{-1} has been used to identify areas with a high likelihood of ET^{29,48,50}. The contours of the 0.25 and 0.5 day^{-1} of the maximum Eady growth rate in the three simulations are similar, but the lines of 0.25 day^{-1} of the $2 \times \text{CO}_2$ and $4 \times \text{CO}_2$ experiments are at a slightly higher latitude than that of PD over the West Pacific and North Atlantic and do not change much over the Southern Hemisphere. In other

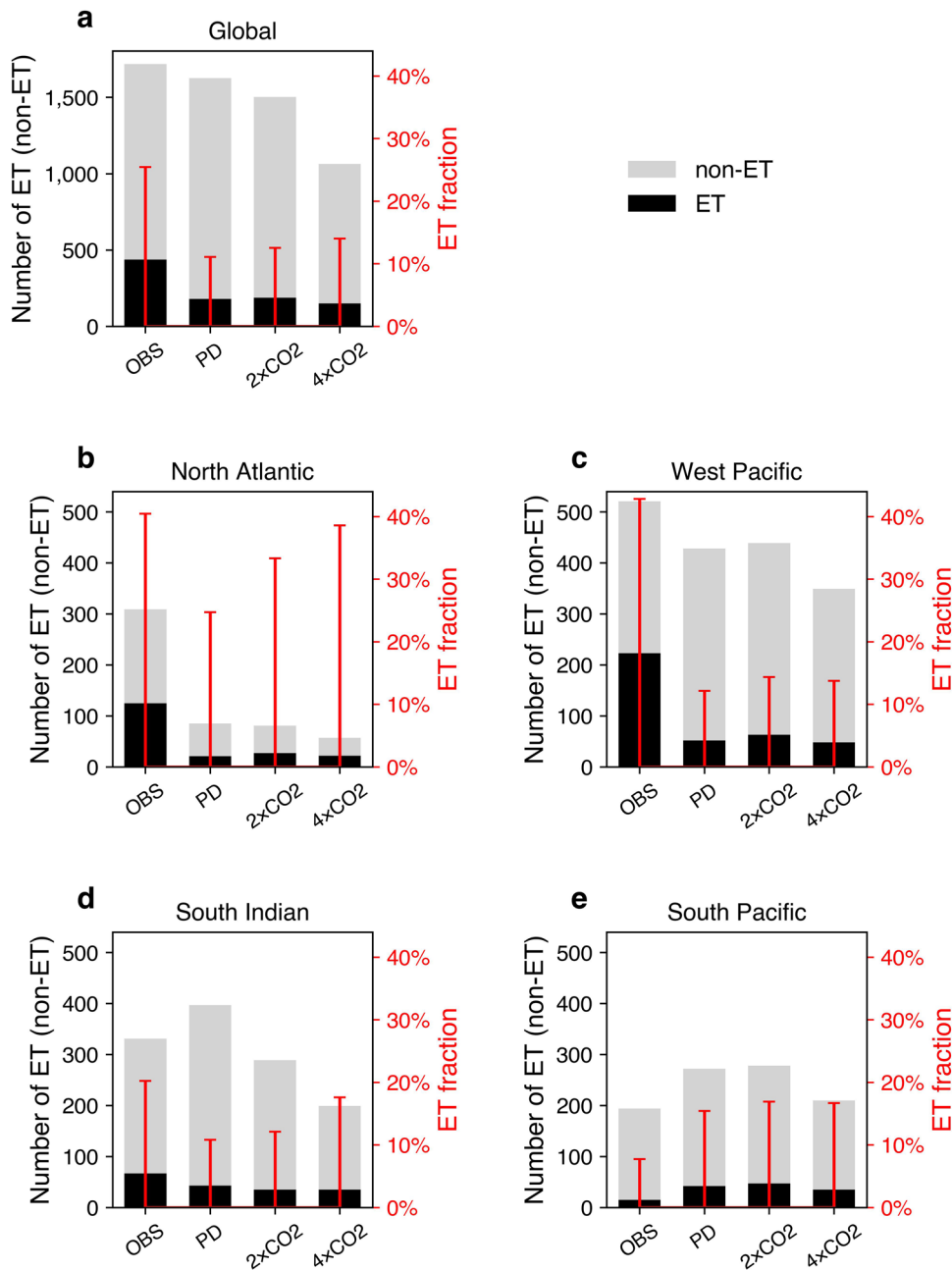


Fig. 3 The number and fraction of extratropical transition (ET) events in a 20-year period. The stacked bar chart represents the number of ET (black) and non-ET (gray) events for the corresponding ocean basin (**a** Global total; **b** North Atlantic; **c** West Pacific; **d** South Indian; **e** South Pacific) and dataset (OBS: IBTrACS; PD: present-day climate simulation; $2\times\text{CO}_2$: doubling CO_2 experiment; $4\times\text{CO}_2$: quadrupling CO_2 experiment), while the stem plot (red vertical line) denotes the ratio of ET events to the total number of tropical cyclones. The number of TC equals the sum of the number of ET and non-ET events.

words, the large-scale environments that promote transition do not alter with increased CO_2 concentration as seen from the spatial distribution of averaged maximum Eady growth rate in the active ET seasons (Supplementary Fig. 2). On the other hand, we observe a greater ET fraction for both $2\times\text{CO}_2$ and $4\times\text{CO}_2$ experiments in the North Atlantic, West Pacific, South Indian, South Pacific, as well as the global total. Since the number of ET events across the three experiments remains similar, the increase in ET fraction can be attributed to the drop in the total number of TCs (or the number of non-ET events).

We also verify whether the latitudes of TC genesis and ET onset would change in response to global warming (Supplementary Fig. 3). Globally, there are poleward shifts in TC genesis and ET onset

latitudes, but not statistically significant, in the $2\times\text{CO}_2$ and $4\times\text{CO}_2$ experiments. In both the North Atlantic and West Pacific, the latitudes of TC genesis and ET onset in the $2\times\text{CO}_2$ and $4\times\text{CO}_2$ experiments are significantly higher than those in the PD (except for the TC genesis in $2\times\text{CO}_2$). In the South Indian and South Pacific, although the two sets of latitudes move poleward in general, the changes are not statistically significant. We can observe from this analysis that the ET onset shifts to slightly higher latitudes or remains in similar latitudes under greenhouse warming in a magnitude comparable to the changes observed in TC genesis. It means that the environment may not be conducive for the number of ET events to increase, which is in agreement with the analysis of the maximum Eady growth rate

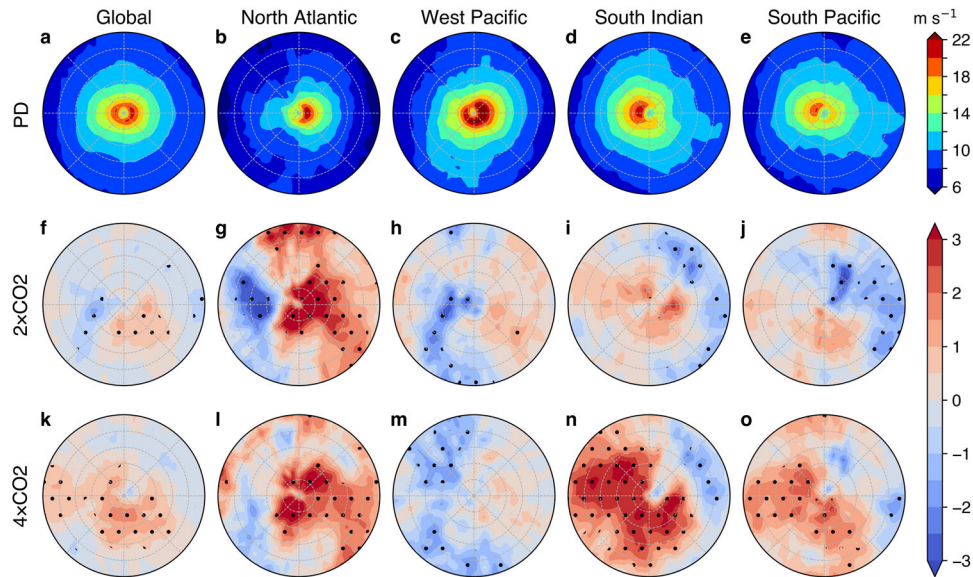


Fig. 4 Compositing 10-m wind speed at the completion of extratropical transition between present-day (PD) climate simulation and increased CO₂ experiments. The radius of each plot is 10°, and the grid (gray line) is drawn in a 2° interval. The top panel (a–e) shows the wind speed interpolated to a storm-centered coordinate of the PD simulation for the global mean, the North Atlantic, West Pacific, South Indian, and South Pacific. The difference in wind speed between the doubling CO₂ experiment (2 × CO₂) and PD is shown in the middle panel (f–j), while that of the quadrupling CO₂ experiment (4 × CO₂) is shown in the bottom panel (k–o). Stippling represents a statistically significant increase or decrease in mean wind speed at a 90% confidence level. Before making the composite, all individual storms were rotated so that their directions of motion were aligned to the north.

(Supplementary Fig. 2). Diverse outcomes for ET onset latitude, however, are observed in other studies. Michaelis and Lackmann³⁰ revealed that the median ET onset latitude would increase in the North Atlantic and remain the same in the West Pacific, but a slight decrease in all basins was detected from ref. ³¹.

In the two elevated CO₂ experiments, we identify a global increase in TC lifetime maximum intensity represented by the 10-m wind speed (Supplementary Fig. 4). Due to its direct link to socioeconomic impacts, wind speed is used as the indicator of TC intensity instead of mean sea level pressure or vorticity. This increase is mainly contributed by the major TCs (i.e., intensity classification greater than Category 3) in the West Pacific and South Indian Ocean. Therefore, it is reasonable to expect that the intensity of a TC at ET completion would be greater when TCs become stronger in the future.

Figure 4 shows the composite 10-m wind speed at the completion of ET events rotated to the direction of storm motion. The inner-core wind speed of the storms is the greatest in the West Pacific and North Atlantic, and the right-hand side of the storm is relatively stronger (Fig. 4b, c). In contrast, the wind speed is higher on the left-hand side for the storms in the Southern Hemisphere (South Indian and South Pacific) (Fig. 4d, e). Globally, there is a mean increase in 10-m wind speed mainly within 6° from the TC center. The increase for the 2 × CO₂ experiment is found in a smaller patch co-exists with a decrease (Fig. 4f), while the increase for the 4 × CO₂ experiment covers a larger area at the rear semicircle (Fig. 4k). For the 2 × CO₂ experiment, the signal of enhanced wind speed is significant in the North Atlantic, where a strong opposite signal exists in smaller area as well (Fig. 4g). Reduced wind speed is primarily noticed in the other basins (Fig. 4h–j). Conversely, we can consistently identify an increase in the North Atlantic, the South Indian, and the South Pacific Ocean in the 4 × CO₂ experiment (Fig. 4l, n, o). A considerable area over the left semicircle of TCs in the South Indian has a higher wind speed. The increase in wind speed can be seen clearly from the mean radial profile (Supplementary Fig. 5). Overall, the strengthening of storms is more pronounced in the 4 × CO₂ experiment than in the 2 × CO₂ experiment. Jung and Lackmann³⁵ explained that the

primary cause of stronger future storms is possibly the higher SST. An increase in SST in the 2 × CO₂ and 4 × CO₂ experiments of the CESM simulations can be seen in Supplementary Fig. 2 of the supplementary information in ref. ²⁴. Similar changes in storm intensity in the North Atlantic and West Pacific at ET completion can be seen from ref. ⁵². An increase in surface wind speed during the transition is also found from the composite of 15 randomized cases of the same event in the North Atlantic³⁵. Furthermore, the increased TC intensity allows TCs to persist longer into the baroclinic zone even if the southward boundary of the baroclinic zone migrates poleward under greenhouse warming.

Change in the destructive potential of transitioned TCs during ETC phase

In addition to intensity, the extent of the wind field that a storm can cover is also an important factor to risk analysis. During ET, the radius of gale-force wind can increase^{4,8}, so a transitioned TC can potentially impact a greater population. An expansion of the 10-m wind field during the ETC phase of transitioned TC is found in the North Atlantic, South Indian, and South Pacific for the 4 × CO₂ experiment, which contributes to a significant increase in the global average (Supplementary Fig. 6). The mean changes observed in the West Pacific are very small.

To comprehensively evaluate the possible damage that a transitioned TC can inflict, we compute the IKE (see “Methods”). It is an alternative metric of the destructive potential of a TC. Unlike the maximum sustained wind speed, which is the common indicator of potential TC impact, IKE considers the wind speed and the extent of the wind field of a TC concurrently. We calculate the IKE of each storm summed over the ETC phase, and classify them into groups of low and high destructive potential. Low and high destructive potential are designated as IKE below the lower quartile (41 TJ) and above the upper quartile (428 TJ) of IKE of the storms in the PD experiment, respectively. For the group of low destructive potential, there is a slight increase in the number of ET events in the 2 × CO₂ experiment but a significant decrease in the 4 × CO₂ experiment over the 20-year period (Supplementary Fig. 7

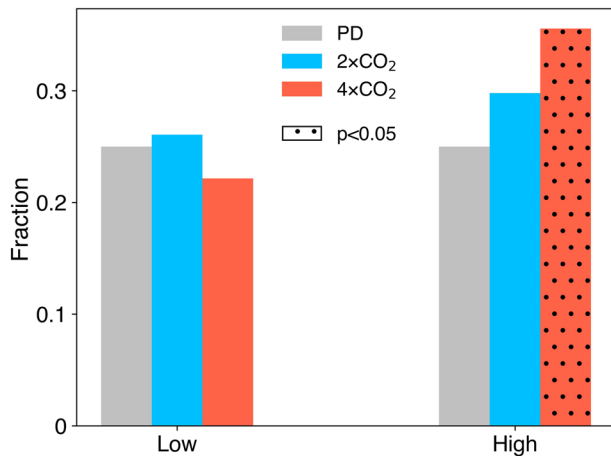


Fig. 5 The proportion of transitioned tropical cyclones with lower and greater destructive potential during their extratropical cyclone phase. A stippled bar indicates an increase or decrease in the proportion of storm in an increased CO₂ experiment (doubling (2×CO₂; blue) and quadrupling CO₂ (4×CO₂; red)) from the present-day simulation (PD; gray) is statistically significant at a 95% confidence level as obtained from the proportion test.

and Supplementary Table 2). These changes in the two sensitivity experiments follow those of total ET events. However, the number of storms in the 2×CO₂ and 4×CO₂ experiments both increase in the group of high destructive potential while only the former one is significant. The increase in the frequency for both low and high group from the 2×CO₂ experiments can explain the indistinct change in the composite wind field (Fig. 4f), as the wind speed of the weaker and stronger storms offset each other. In terms of change in fraction, we only detect a minor increase and decrease for the 2×CO₂ and 4×CO₂ experiments, respectively, in the group of low destructive potential (Fig. 5). For the group of high destructive potential, we identify a greater fraction in both sensitivity experiments, while the increase for the 4×CO₂ experiment is significant. In summary, there are larger number (for 2×CO₂) or fraction (for 4×CO₂) of ETCs originated from the tropics with greater destructive potential under greenhouse warming.

DISCUSSION

We analyze the climate simulations from a fully coupled Earth System model (CESM) with high resolutions in the atmosphere and ocean components to examine potential changes in ET activities and associated destructive potential under greenhouse warming. The two different CO₂ concentration scenarios give similar conclusions: when CO₂ concentration is doubled, the transitioned TCs are not significantly stronger than those in the present-day climate on average. There are more ETCs with both lower and higher destructive potential, while the increase for the latter group is significant. When CO₂ concentration is quadrupled, the storms are stronger. Although there are fewer ET events in total, the ETCs with higher destructive potential have a significant increase in proportion. In both cases, we can expect a greater impact from the transitioned TCs on the mid-latitude region due to human-induced global warming. The results for the North Atlantic (greater ET fraction and intensity in both the 2×CO₂ and 4×CO₂ experiments) broadly consistent with other studies^{29–31,33,34}.

Since an ET event cannot develop without a TC form in the first place, we can expect the uncertainty of the prediction of ET largely inherits from that of TC activity. Reliable ET statistics in a simulation depend on the maximum TC intensity a model can

produce, as weaker model storms may not be able to survive long enough until ET can start. Although finer model resolution shows improved ability in simulating very intense TC⁴⁴, it is still underestimated in our model as seen in Supplementary Fig. 8. While most of the TCs in the model are developed to up to Category 2 ($\leq 49 \text{ m s}^{-1}$), only 8.3% of them are major TCs and none of them can become a Category 5 storm ($>70 \text{ m s}^{-1}$). It explains why the model in the current study underestimates the overall number of ET events in the present-day climate simulation, especially in the West Pacific. In this basin, only a small fraction of TCs can transform to ETCs relative to the observation (Fig. 3c). Haarsma⁵³ suggests that an atmosphere-ocean coupled model with horizontal resolution of at least 10 km, which is finer than most of the state-of-the-art Earth system models at present, is necessary for such purpose. Meanwhile, simulated TC genesis can directly influence the number of ET events. The lack of model TC formed in the North Atlantic, which may be due to biases in convective activity, easterly wave, or SST²⁴, is likely to be the cause of the low bias of ET events in the region.

The actual distributions of TC intensity and track in the greenhouse warming experiments are highly uncertain given the large bias in TC frequency in the North Atlantic. Furthermore, the bias differs for TC tracks that are favorable (those moving poleward) and unfavorable to ET (those moving toward the Gulf of Mexico). Thus, the ET uncertainty results from the TC uncertainty (rather than the baroclinic environment) can be quite large. On the other hand, we can expect a smaller uncertainty in ET activity in the West Pacific because of a smaller bias in TC frequency. It is desirable to use ensemble model to quantify the model uncertainty. However, performing multiple sets of fully coupled climate simulations at high resolution is extremely expensive and unfeasible. A collaborative effort to produce simulations from different models is required to obtain a more comprehensive picture of risk caused by ET events.

Despite lower occurrence than TCs, ETCs originated from the tropics should not be taken lightly due to their larger coverage^{4,8}, which allows far-reaching impact. Our results provide a scientific basis for building climate resilience in the mid-latitude regions to combat the risk caused by climate-related hazards under anthropogenic climate change. It is especially important for the coastal populations which are more vulnerable to compound hazards including high wind and flooding caused by extreme rainfall and/or storm surge.

METHODS

Historical TC data and model outputs

We use the best track of IBTrACS⁴³ for the period 1991–2010. This dataset contains the observation from the forecast agencies in their respective area of responsibility at six-hourly intervals. The center location (latitude and longitude) of TCs that is used in the present study is the average from all the available sources. An ET event is defined based on the variable “nature” in the dataset. The maximum sustained wind speed is obtained from the variable “usa_wind”.

The CESM v1.2.2 is a fully coupled global climate model that includes various components of the Earth system⁵⁴. The component set is BC5: the atmosphere, ocean, land, and sea ice components are the Community Atmosphere Model version 5 (CAM5), the Parallel Ocean Program version 2 (POP2), the Community Land Model version 4 (CLM4), and the Community Ice Code version 4 (CICE4), respectively. The grid resolution is ne120_t12: CAM5 and CLM4 have a horizontal resolution of 0.25°, while that of POP2 and CICE4 are 0.1°. The number of vertical levels in CAM5 and POP2 are 30 and 62, respectively. The three experiments differ in the level of CO₂ concentration, while the level of other greenhouse gases and aerosols are the same as in

the PD experiment. The prescribed CO₂ concentration for the PD, 2 × CO₂, and 4 × CO₂ experiments are 367 ppm, 734 ppm, and 1468 ppm, respectively. The PD experiment is integrated for 140 years after initialization from a quasi-equilibrated climate state. The 2 × CO₂ and 4 × CO₂ experiments start at year 71 of the PD experiment and are integrated for 100 years further. The elevated CO₂ concentration in the 2 × CO₂ and 4 × CO₂ experiments are prescribed abruptly so that it would take up to several hundreds of years to attain complete equilibrium. As a compromise, we utilize the last 20 years of these two experiments to represent a better-equilibrated state. The 4 × CO₂ experiment is introduced to identify whether there is a nonlinearity in the climate response to CO₂ forcing. The strong anthropogenic forcing of the 4 × CO₂ scenario can also allow us to distinguish its impact from the natural variability of the climate on the change of ET events. Details of the experiments are explained in ref. ²⁴.

Detection and tracking of model TCs

The TCs in the model are detected and tracked at six-hourly interval using the same method as in ref. ²⁴, which is largely based on the one applied in ref. ⁵⁵. It is a simple algorithm which only uses surface pressure, 10-m wind speed, and surface vorticity because only a limited number of variables are produced at a six-hourly interval. For vortex detection, the global field of the departure of six-hourly surface pressure from the 14-day retrospective mean is first calculated for all time steps. A vortex is regarded as a TC candidate if (1) it is a local minimum in the surface pressure anomaly field with a difference of at least 3 hPa from the neighboring grid points, and (2) the maximum value of the 10-m wind speed within 100 km from the vortex center exceeds 10 m s⁻¹, and (3) the surface vorticity is greater than 0.00145 s⁻¹. For tracking, the procedure for the second time step (time $t + 6$ h) differs from that for the subsequent time steps (time $t + 12$ h and beyond) of each potential track. A vortex at any time t is connected to the one at time $t + 6$ h that is closest to it and a potential track is formed. For time $t + 12$ h, a first estimate is computed by extrapolating from the vortex location in the previous two time steps. The vortex at time $t + 12$ h which is closest to the first estimate and is within 400 km from the vortex at the previous time step is added to the same track. The procedure for time $t + 12$ h is repeated for subsequent time steps. Whenever a vortex cannot be found within 400 km from the location at the previous time step of a track, the tracking is discontinued. We remove tracks which are duplicate, or have a maximum 10-m wind speed less than 17 m s⁻¹, or survive for less than 2 days.

Cyclone phase space

The cyclone phase space is a framework depicting the evolution of the structure of a TC⁵⁶. It has been used in many studies for objectively and automatically defining ET events on gridded datasets^{29,33,46,47}. A main advantage of this framework is that it can be conveniently computed using geopotential height at several pressure levels. For each time step, two parameters are calculated, namely B and $-V_T^L$. The parameter B indicates the existence of the frontal nature (or symmetry) of a cyclone and is defined as the storm-motion-relative 900–600-hPa thickness asymmetry across it. It is computed using the formula

$$B = h(\overline{Z_{600\text{ hPa}} - Z_{900\text{ hPa}}}_{\text{right}} - \overline{Z_{600\text{ hPa}} - Z_{900\text{ hPa}}}_{\text{left}}) \quad (1)$$

where Z is the geopotential height, h is a value indicating the hemisphere in which the TC is located (1 for the Northern Hemisphere and -1 for the Southern Hemisphere), an overbar means that the value underneath is taken average within 500 km on the left/right-hand side of the TC. On the other hand, the parameter $-V_T^L$ indicates the presence of warm-core or cold-core vertical structure and is defined as the vertical derivative of

horizontal geopotential height gradient in the lower troposphere. It is computed using the formula

$$-V_T^L = \frac{\partial(\Delta Z)}{\partial \ln p} \Big|_{900\text{ hPa}}^{600\text{ hPa}} \quad (2)$$

where ΔZ is the geopotential height perturbation (Z_{max} minus Z_{min}) calculated within 500 km of the TC center, and p is the pressure level (either 600 or 900 hPa). To minimize the impact of short-term fluctuation on the result, smoothing using a five-point running average is applied to both parameters. The missing values at the beginning and end of the time series of the two parameters (resulted from the running average) are filled with the corresponding unsmoothed values.

Since TCs have a high degree of symmetry with a warm-core structure, they have small B values and positive $-V_T^L$ values. However, ETCs are highly asymmetry and have a cold-core, they have large B values with $-V_T^L$ in the negative range. In this study, the threshold of B for classifying symmetric and asymmetric storms is set to 15, following ref. ⁴⁶. As ET is a process by which a TC becomes an ETC, the ET onset can be defined as the first time step at which a TC (a) becomes asymmetric ($B > 15$) or (b) acquires cold-core structure ($-V_T^L < 0$). These two pathways of ET have also been considered in various studies^{29,33,46,47}. By the same token, the first time step at which a TC develops into a storm with asymmetry and cold-core structure after an onset is regarded as ET completion.

We exclude the model TCs that do not pass through the right bottom quadrant in the cyclone phase space throughout their life cycles, because it means that they do not possess tropical characteristics to be a TC. There are 74, 80, and 93 such TCs in the PD, 2 × CO₂, and 4 × CO₂ experiments, respectively.

Maximum Eady growth rate

The maximum Eady growth rate indicates the baroclinic instability which is used for determining whether an environment is favorable to ET. Hoskins and Valdes used this parameter to represent baroclinically active regions⁵⁷. It has been used for indicating regions of high likeliness of ET when values greater than 0.25 day⁻¹ (see refs. ^{29,48,50}). The parameter is defined as $\sigma = 0.31fN^{-1} dU/dz$, where f is the Coriolis parameter, N is the Brunt–Väisälä frequency at 700 hPa, $dU(u,v)/dz$ is the vertical wind shear between 200 hPa and 850 hPa, $U(u,v)$ is the wind speed, and z is the geometric height.

Integrated kinetic energy

Following Powell and Reinhold⁵⁸, integrated kinetic energy at a time step is defined as

$$IKE = \int_V \frac{1}{2} \rho U^2 dV = \frac{1}{2} \int_A U^2 dA \quad (3)$$

where ρ is the air density ($=1 \text{ kg m}^{-3}$), U is the 10-m wind speed field, and V and A denote volume and area, respectively. In the present study, IKE is calculated using the grid points with U greater than 18 m s⁻¹ within 1000 km from the TC center.

Significance test

The significance of changes in 10-m wind speed or area from PD to 2 × CO₂ (4 × CO₂) experiments is determined by one-tailed independent samples Welch's t test, which is similar to Student's t test but does not assume equal variance between two populations. For the comparison of the proportion of destructive ETCs, the two-sample one-tailed Z test for proportion⁵⁹ is employed. We use the one-tailed Mann–Whitney U test, which is a nonparametric test, for checking any change in the annual number of ET events in the 20-year period.

DATA AVAILABILITY

The best track data of the IBTrACS are available at <https://www.ncei.noaa.gov/products/international-best-track-archive>. The CESM model output can be requested at <https://ibscclimate.org/research/ultra-high-resolution-climate-simulation-project>.

CODE AVAILABILITY

Codes are available upon request. Figures are generated by Python 3.10.6 (Matplotlib 3.6, Basemap 1.3.4).

Received: 7 April 2023; Accepted: 25 August 2023;

Published online: 09 September 2023

REFERENCES

- Klein, P. M., Harr, P. A. & Elsberry, R. L. Extratropical transition of western North Pacific tropical cyclones: an overview and conceptual model of the transformation stage. *Weather Forecast.* **15**, 373–395 (2000).
- Harr, P. A. & Elsberry, R. L. Extratropical transition of tropical cyclones over the western North Pacific. Part I: evolution of structural characteristics during the transition process. *Mon. Weather Rev.* **128**, 2613–2633 (2000).
- Harr, P. A., Elsberry, R. L. & Hogan, T. F. Extratropical transition of tropical cyclones over the western North Pacific. Part II: the impact of midlatitude circulation characteristics. *Mon. Weather Rev.* **128**, 2634–2653 (2000).
- Jones, S. C. et al. The extratropical transition of tropical cyclones: forecast challenges, current understanding, and future directions. *Weather Forecast.* **18**, 1052–1092 (2003).
- Evans, C. et al. The extratropical transition of tropical cyclones. Part I: cyclone evolution and direct impacts. *Mon. Weather Rev.* **145**, 4317–4344 (2017).
- Sekioka, M. A hypothesis on complex of tropical and extratropical cyclones for typhoon in the middle latitudes. *J. Meteorol. Soc. Jpn.* **35**, 170–173 (1957).
- Palmén, E. Vertical circulation and release of kinetic energy during the development of Hurricane Hazel into an extratropical storm. *Tellus* **10**, 1–13 (1958).
- Evans, C. & Hart, R. E. Analysis of the wind field evolution associated with the extratropical transition of Bonnie (1998). *Mon. Weather Rev.* **136**, 2047–2065 (2008).
- Sainsbury, E. M. et al. How important are post-tropical cyclones for European windstorm risk? *Geophys. Res. Lett.* **47**, e2020GL089853 (2020).
- Keller, J. H. et al. The extratropical transition of tropical cyclones. Part II: interaction with the midlatitude flow, downstream impacts, and implications for predictability. *Mon. Weather Rev.* **147**, 1077–1106 (2019).
- Halverson, J. B. & Rabenhorst, T. Hurricane Sandy: the science and impacts of a superstorm. *Weatherwise* **66**, 14–23 (2013).
- Kantha, L. Classification of hurricanes: lessons from Katrina, Ike, Irene, Isaac and Sandy. *Ocean. Eng.* **70**, 124–128 (2013).
- Galarneau, T. J., Davis, C. A. & Shapiro, M. A. Intensification of Hurricane Sandy (2012) through extratropical warm core occlusion. *Mon. Weather Rev.* **141**, 4296–4321 (2013).
- Moore, P. An analysis of storm Ophelia which struck Ireland on 16 October 2017. *Weather* **76**, 301–306 (2021).
- Rantanen, M., Räisänen, J., Sinclair, V. A. & Lento, J. The extratropical transition of Hurricane Ophelia (2017) as diagnosed with a generalized omega equation and vorticity equation. *Tellus* **72**, 1–26 (2020).
- Yanase, W. et al. Multiple dynamics of precipitation concentrated on the north side of Typhoon Hagibis (2019) during extratropical transition. *J. Meteorol. Soc. Jpn.* **100**, 783–805 (2022).
- Takemi, T. & Unuma, T. Environmental factors for the development of heavy rainfall in the eastern part of Japan during Typhoon Hagibis (2019). *Sci. Online Lett. Atmos.* **16**, 30–36 (2020).
- Moya, L., Mas, E. & Koshimura, S. Learning from the 2018 western Japan heavy rains to detect floods during the 2019 Hagibis Typhoon. *Remote Sens.* **12**, 2244 (2020).
- Ribeiro, S. L., Gonçalves, A., Cascarejo, I., Liberato, M. L. R. & Fonseca, T. F. Development of a catalogue of damage in Portuguese forest associated with extreme extratropical cyclones. *Sci. Total Environ.* **814**, 151948 (2022).
- Laurila, T. K., Sinclair, V. A. & Gregow, H. The extratropical transition of Hurricane Debby (1982) and the subsequent development of an intense windstorm over Finland. *Mon. Weather Rev.* **148**, 377–401 (2020).
- Adams, K. & Heidarzadeh, M. Extratropical cyclone damage to the seawall in Dawlish, UK: eyewitness accounts, sea level analysis and numerical modelling. *Nat. Hazards* **116**, 637–662 (2023).
- Rezaee, S., Pelot, R. & Finnis, J. The effect of extratropical cyclone weather conditions on fishing vessel incidents' severity level in Atlantic Canada. *Saf. Sci.* **85**, 33–40 (2016).
- Tochimoto, E., Yokota, S., Niino, H. & Yanase, W. Mesoscale convective vortex that causes tornado-like vortices over the sea: a potential risk to maritime traffic. *Mon. Weather Rev.* **147**, 1989–2007 (2019).
- Chu, J.-E. et al. Reduced tropical cyclone densities and ocean effects due to anthropogenic greenhouse warming. *Sci. Adv.* **6**, eabd5109 (2020).
- Knutson, T. et al. Tropical cyclones and climate change assessment: Part II: projected response to anthropogenic warming. *Bull. Am. Meteorol. Soc.* **101**, E303–E322 (2020).
- Sobel, A. H. et al. Human influence on tropical cyclone intensity. *Science* **353**, 242–246 (2016).
- Emanuel, K. Response of global tropical cyclone activity to increasing CO₂: results from downscaling CMIP6 models. *J. Clim.* **34**, 57–70 (2021).
- Bhatia, K., Vecchi, G., Murakami, H., Underwood, S. & Kossin, J. Projected response of tropical cyclone intensity and intensification in a global climate model. *J. Clim.* **31**, 8281–8303 (2018).
- Liu, M., Vecchi, G. A., Smith, J. A. & Murakami, H. The present-day simulation and twenty-first-century projection of the climatology of extratropical transition in the North Atlantic. *J. Clim.* **30**, 2739–2756 (2017).
- Michaelis, A. C. & Lackmann, G. M. Climatological changes in the extratropical transition of tropical cyclones in high-resolution global simulations. *J. Clim.* **32**, 8733–8753 (2019).
- Bieli, M., Sobel, A. H., Camargo, S. J., Murakami, H. & Vecchi, G. A. Application of the cyclone phase space to extratropical transition in a global climate model. *J. Adv. Model. Earth Syst.* **12**, e2019MS001878 (2020).
- Haarsma, R. J. et al. High resolution model intercomparison project (HighResMIP v1.0) for CMIP6. *Geosci. Model Dev.* **9**, 4185–4208 (2016).
- Baker, A. J. et al. Extratropical transition of tropical cyclones in a multiresolution ensemble of atmosphere-only and fully coupled global climate models. *J. Clim.* **35**, 5283–5306 (2022).
- Jung, C. & Lackmann, G. M. The response of extratropical transition of tropical cyclones to climate change: quasi-idealized numerical experiments. *J. Clim.* **34**, 4361–4381 (2021).
- Jung, C. & Lackmann, G. M. Changes in tropical cyclones undergoing extratropical transition in a warming climate: Quasi-idealized numerical experiments of North Atlantic landfalling events. *Geophys. Res. Lett.* **50**, e2022GL101963 (2023).
- Sainsbury, E. M. et al. Can low-resolution CMIP6 ScenarioMIP models provide insight into future European post-tropical-cyclone risk? *Weather Clim. Dyn.* **3**, 1359–1379 (2022).
- Roberts, M. J. et al. Impact of model resolution on tropical cyclone simulation using the HighResMIP-PRIMAVERA multimodel ensemble. *J. Clim.* **33**, 2557–2583 (2020).
- Lok, C. C. F., Chan, J. C. L. & Toumi, R. Importance of air-sea coupling in simulating tropical cyclone intensity at landfall. *Adv. Atmos. Sci.* **39**, 1777–1786 (2022).
- Li, H. & Srivier, R. L. Tropical cyclone activity in the high-resolution Community Earth System Model and the impact of ocean coupling. *J. Adv. Model. Earth Syst.* **10**, 165–186 (2018).
- Emanuel, K. A. An air-sea interaction theory for tropical cyclones. Part I: steady-state maintenance. *J. Atmos. Sci.* **43**, 585–605 (1986).
- Schade, L. R. & Emanuel, K. A. The ocean's effect on the intensity of tropical cyclones: results from a simple coupled atmosphere–ocean model. *J. Atmos. Sci.* **56**, 642–651 (1999).
- Vecchi, G. A. et al. Tropical cyclone sensitivities to CO₂ doubling: roles of atmospheric resolution, synoptic variability and background climate changes. *Clim. Dyn.* **53**, 5999–6033 (2019).
- Knapp, K. R., Kruk, M. C., Levinson, D. H., Diamond, H. J. & Neumann, C. J. The international best track archive for climate stewardship (IBTrACS): unifying tropical cyclone data. *Bull. Am. Meteorol. Soc.* **91**, 363–376 (2010).
- Murakami, H. et al. Simulation and prediction of category 4 and 5 hurricanes in the high-resolution GFDL HiFLOR coupled climate model. *J. Clim.* **28**, 9058–9079 (2015).
- Bacmeister, J. T. et al. Projected changes in tropical cyclone activity under future warming scenarios using a high-resolution climate model. *Clim. Change* **146**, 547–560 (2018).
- Zarzycki, C. M., Thatcher, D. R. & Jablonowski, C. Objective tropical cyclone extratropical transition detection in high-resolution reanalysis and climate model data. *J. Adv. Model. Earth Syst.* **9**, 130–148 (2017).
- Bieli, M., Camargo, S. J., Sobel, A. H., Evans, J. L. & Hall, T. A global climatology of extratropical transition. Part I: characteristics across basins. *J. Clim.* **32**, 3557–3582 (2019).
- Hart, R. E. & Evans, J. L. A climatology of the extratropical transition of Atlantic tropical cyclones. *J. Clim.* **14**, 546–564 (2001).
- Studholme, J., Hodges, K. I. & Brierley, C. M. Objective determination of the extratropical transition of tropical cyclones in the Northern Hemisphere. *Tellus* **67**, 24474 (2015).
- Kitabatake, N. Climatology of extratropical transition of tropical cyclones in the western North Pacific defined by using cyclone phase space. *J. Meteorol. Soc. Jpn.* **89**, 309–325 (2011).

51. Roberts, M. J. et al. Projected future changes in tropical cyclones using the CMIP6 HighResMIP multimodel ensemble. *Geophys. Res. Lett.* **47**, e2020GL088662 (2020).
52. Michaelis, A. C. & Lackmann, G. M. Storm-scale dynamical changes of extra-tropical transition events in present-day and future high-resolution global simulations. *J. Clim.* **34**, 5037–5062 (2021).
53. Haarsma, R. European windstorm risk of post-tropical cyclones and the impact of climate change. *Geophys. Res. Lett.* **48**, e2020GL091483 (2021).
54. Small, R. J. et al. A new synoptic scale resolving global climate simulation using the Community Earth System Model. *J. Adv. Model. Earth Syst.* **6**, 1065–1094 (2014).
55. Bacmeister, J. T. et al. Exploratory high-resolution climate simulations using the Community Atmosphere Model (CAM). *J. Clim.* **27**, 3073–3099 (2014).
56. Hart, R. E. A cyclone phase space derived from thermal wind and thermal asymmetry. *Mon. Weather Rev.* **131**, 585–616 (2003).
57. Hoskins, B. J. & Valdes, P. J. On the existence of storm-tracks. *J. Atmos. Sci.* **47**, 1854–1864 (1990).
58. Powell, M. D. & Reinhold, T. A. Tropical cyclone destructive potential by integrated kinetic energy. *Bull. Am. Meteorol. Soc.* **88**, 513–526 (2007).
59. Yadav, S. K., Singh, S. & Gupta, R. Test for inference: categorical data I. in *Biomedical Statistics: A Beginner's Guide* (eds Yadav, S. K., Singh, S. & Gupta, R.) 115–119 (Springer, 2019).

ACKNOWLEDGEMENTS

This research was supported City University of Hong Kong under project number 9610571.

AUTHOR CONTRIBUTIONS

J.-E.C. conceived the idea, designed the study, downloaded, and extracted the model data, and performed the model TC detection and tracking. H.M.C. conducted the data analysis, prepared the figures, and drafted and wrote the manuscript. H.M.C. and J.-E.C. reviewed and edited the manuscript.

COMPETING INTERESTS

The authors declare no competing interests.

ADDITIONAL INFORMATION

Supplementary information The online version contains supplementary material available at <https://doi.org/10.1038/s41612-023-00470-8>.

Correspondence and requests for materials should be addressed to Jung-Eun Chu.

Reprints and permission information is available at <http://www.nature.com/reprints>

Publisher's note Springer Nature remains neutral with regard to jurisdictional claims in published maps and institutional affiliations.



Open Access This article is licensed under a Creative Commons Attribution 4.0 International License, which permits use, sharing, adaptation, distribution and reproduction in any medium or format, as long as you give appropriate credit to the original author(s) and the source, provide a link to the Creative Commons license, and indicate if changes were made. The images or other third party material in this article are included in the article's Creative Commons license, unless indicated otherwise in a credit line to the material. If material is not included in the article's Creative Commons license and your intended use is not permitted by statutory regulation or exceeds the permitted use, you will need to obtain permission directly from the copyright holder. To view a copy of this license, visit <http://creativecommons.org/licenses/by/4.0/>.

© The Author(s) 2023